Electron backscatter diffraction characterisation of liquid route processed Ti6242S/SCS-6 composites

Carine Duda, Anne-Françoise Gourgues

Electron backscatter diffraction characterisation of liquid route processed Ti6242S/SCS-6 composites

Carine Duda [a], Anne-Françoise Gourgues [b]

[a] *Institut de Chimie de la Matière Condensée de Bordeaux (ICMCB-CNRS), 87 avenue du Docteur Schweitzer, 33608 Pessac Cedex, France*
[b] *Ecole Nationale Supérieure des Mines de Paris, Centre des Matériaux P.M. Fourt, UMR CNRS 7633, BP87, 91003 Evry Cedex, France*

Abstract : Liquid route processed filamentary titanium matrix composites reinforced by ceramic filaments were investigated using electron backscatter diffraction and high resolution scanning electron microscopy. As-processed filamentary materials possess a metastable microstructure with martensitic α + retained β matrix and small sub-stoichiometric TiC_{1-x} precipitates at the fibre/matrix interface. The heat treatment induced morphological and crystallographic modification of carbides and coarsening of the matrix. The analysis method was also used to validate a simulation route to obtain bulk materials having similar microstructural properties.

1. Introduction

Incorporation of reinforcing ceramic filaments in titanium alloys seems to be highly promising for aircraft applications. For several decades, the manufacturing processes of titanium matrix composites have been based on fibre/foil/fibre method, plasma spray coating and physical vapour deposition routes. However, the excessive costs of these processes have limited industrial development of these materials. An alternative method has been recently developed. The liquid route process, followed by rapid cooling, allows obtaining filamentary composites consisting in silicon carbide filaments and titanium alloy coating at reasonable costs. In order to model the mechanical properties of the as-processed titanium matrix composites (TMC) for aircraft engine applications, filament/matrix interactions must be studied. The present contribution aims at pointing out the local crystallographic properties of the filament/matrix interface and Ti alloy fine-scale microstructure in as processed and in heat-treated filamentary composites.

* Corresponding author. Tel.: +33 1 60 76 30 66; fax: +33 1 60 76 31 50.
E-mail addresses: carine.duda@wanadoo.fr (C. Duda), anne-francoise.gourgues@ensmp.fr (A.-F. Gourgues).
[1] Tel.: +33 6 81 67 37 91.

To investigate phase transformations occurring during processing of materials, the electron backscatter diffraction (EBSD) technique can be used to depict grain orientation, misorientations between grains, texture inheritance, variant selection and to determine the parent phase orientation with much easier sample preparation than for transmission electron microscopy (TEM) (e.g. [1,2]).

Titanium alloys may present two allotropic phases: a high temperature body centred cubic (bcc) β phase and a low temperature hexagonal close-packed (hcp) α phase. The β → α phase transformation is generally governed by the Burgers orientation relationships between α and β phases. EBSD studies have been carried out on the crystallographic phenomena dealing with phase transformation in Ti alloys, such as texture evolution [3,4], crystallographic variant selection [5-8] or habit plane determination [9–11]. These works emphasized correlations between manufacturing process and variant selection associated to β → α phase transformation [6,12] on bulk titanium alloys. Ti6242S titanium alloy reinforced by SiC filaments has been investigated with EBSD [13], focused on the local matrix texture resulting from viscoplastic matrix flow during the fibre/foil/fibre processing route, but not on phase transformations.

This paper deals with EBSD analyses of SiC_{CVD} single filaments coated with Ti6242S titanium alloy via the liquid processing route. Three types of materials have been examined: as processed SiC/Ti6242S filamentary materials, heat treated

filamentary TMCs and simulated materials (rapidly solidified mix of Ti6242S alloy and carbon powder), which could provide a model of filamentary materials. Interactions between the carbon outer layer of the ceramic filament and the Ti6242S alloy, related to the high reactivity of Ti with C at high temperature, are discussed in view of the Ti–C phase diagram as long as the corresponding Ti6242S–C phase diagram is not available in literature and as alloying elements probably play a minor role in the involved phase transformations mechanisms.

2. Experimental procedures

2.1. Materials

The Ti6242S titanium alloy matrix used in the present study is an $\alpha+\beta$ forged alloy having the following chemical composition: Ti–6Al–2Sn–4Zr–2Mo–0.1Si (wt.%). Its microstructure consists of primary equiaxed α grains (80–90 vol.%) in a partially transformed β matrix (Fig. 1a). In this alloy, aluminium is an efficient α-stabiliser, whereas β-stabiliser molybdenum moderates the effect of aluminium. A low amount of silicon has been added to improve creep resistance.

The SiC_{CVD} single filaments used for manufacturing the SiC/Ti alloy filamentary titanium matrix composites (TMC) are 140 μm in diameter SCS-6 Textron® fibres. Tailoring the fibre surface for protecting the SiC filament against chemical aggression and above all against micro defect propagation led the manufacturer to complete the SiC chemical vapour deposition (CVD) on a carbon core by an additional coating, consisting of SiC containing carbon layers, whose total thickness is about 3 μm, and which exhibits compositional gradient in silicon content.

The filamentary TMC manufacturing process consists in running the SiC_{CVD} filaments at very high speed (>1 m s^{-1}) in levitating liquid titanium alloy [14] before rapid cooling by a specific device. The short time contact of some tenths of a second between the C + SiC coated SiC filaments and the liquid Ti6242S alloy induces some chemical interactions related to the

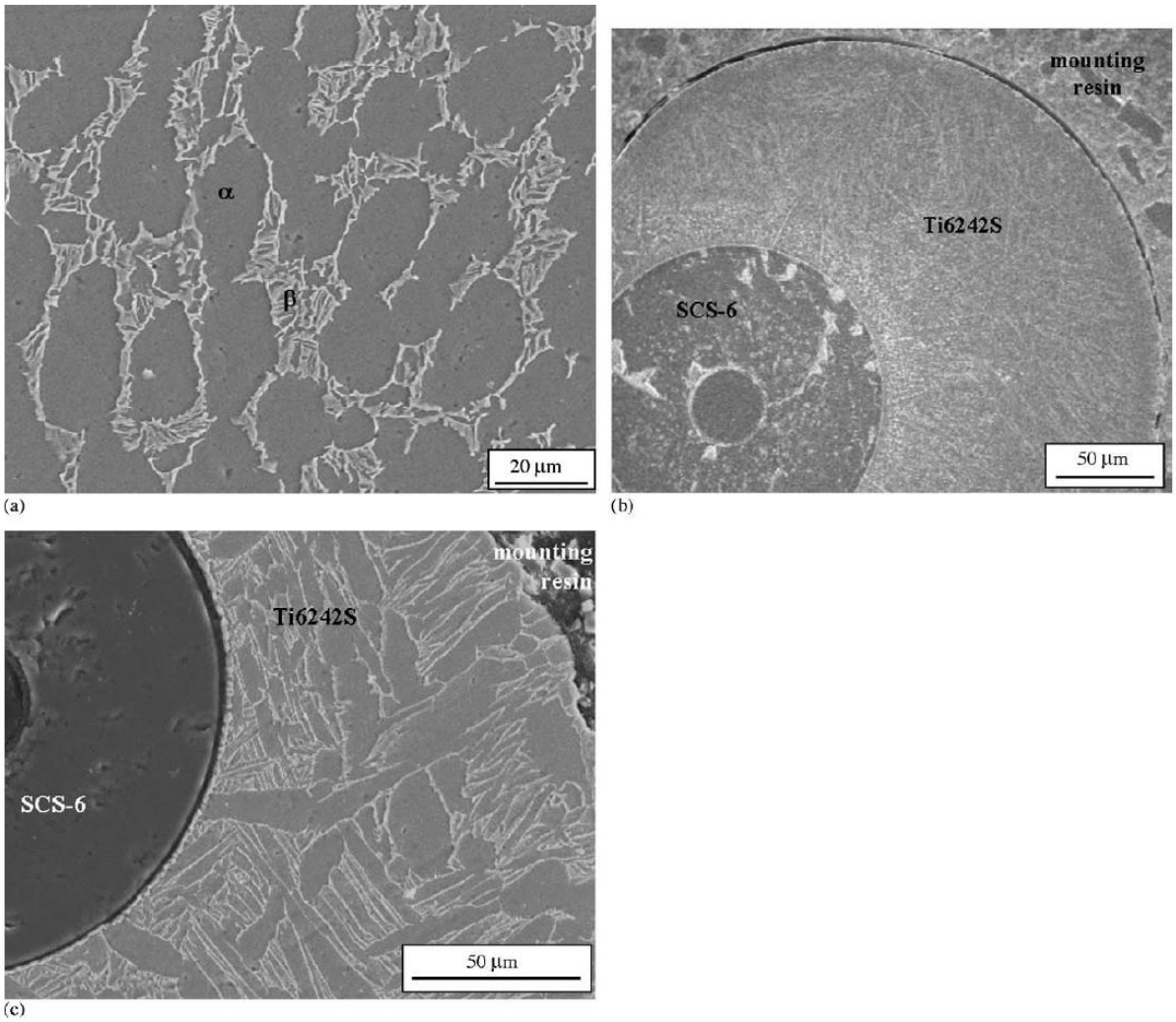

Fig. 1. Microstructure of materials (SEM, secondary electron imaging): (a) bulk $\alpha+\beta$ forged Ti6242S; (b) as-processed filamentary material; (c) heat treated filamentary material.

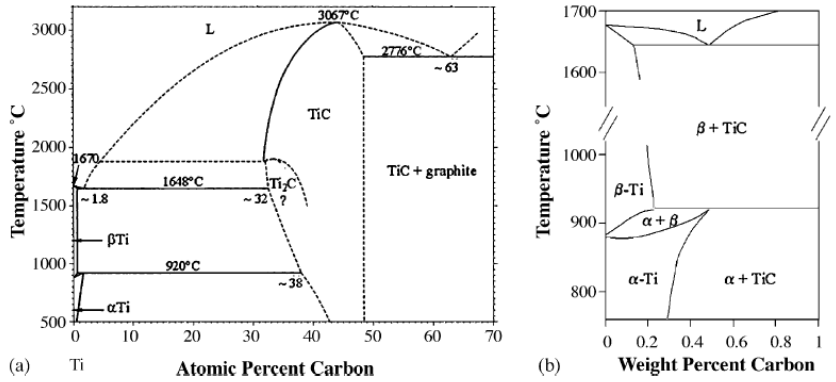

Fig. 2. (a) General and (b) closer view of the Ti-rich side of the Ti–C equilibrium phase diagram (after [15]).

transfer of chemical species and more particularly that of carbon, which may induce unfavourable microstructures. To analyse the effects of consolidation thermal cycle on filament/matrix interactions, post processing isothermal treatments were performed on filamentary TMCs. These were treated at around 950 °C for more than 1 h under purified argon in a radio frequency heated titanium furnace simultaneously used as interstitial getter.

Moreover, in order to reproduce the cooling conditions undergone by the Ti6242S alloy during the liquid route process of filamentary TMCs, but over a more extended volume, a mix of α + β forged Ti6242S and carbon powder was manufactured by arc melting under purified argon flow, and then by cooling by contact with a 15 mm thick, water-cooled copper substrate. The carbon concentration of this simulated material was set to 0.25 wt.%. According to the binary titanium/carbon phase diagram (Fig. 2) [15], this concentration corresponds at high temperature to equilibrium between titanium and carbide precipitated phase, and at intermediate temperature to α + β titanium-based solid solution.

2.2. Investigation methods

The various microstructures were investigated by using a LEO DSM 982 Gemini scanning electron microscope (SEM) equipped with a field emission gun (FEG). Cross-sections of the filamentary TMC specimens were prepared by polishing with diamond paste and with a colloidal silica finish to remove damage induced by mechanical polishing. In addition, the α and β phases, as well as the reaction products near the fibre/matrix interface were revealed by this preparation technique. Standardless X-ray energy dispersive spectroscopy (EDS) analyses were performed at 9 mm working distance and with high voltage of 20 kV, whereas high-resolution images were obtained at 5 kV with a working distance of 3 mm.

To investigate local crystallographic orientations, electron backscatter diffraction (OIM® 2.7 system) was performed with a sample tilt of 70°, a 20 kV high voltage, a working distance of 19 mm and a probe current of 0.1 nA. Crystallographic features of the various phases were characterised using point measurements.

3. Crystallographic background

3.1. Orientation relationships between α and β phases

The two allotropic α (hcp) and β (bcc) phases of titanium are generally linked together by the Burgers orientation relationships (e.g. [9,12]), which correspond to e.g. $(1\,1\,0)_\beta // (0\,0\,0\,1)_\alpha$ and $[1\,\bar{1}\,1]_\beta // [1\,1\,\bar{2}\,0]_\alpha$. According to the symmetry elements of both phases, the theoretical number of inherited α variants from a given parent β grain is equal to 12 [5,7]. In fact, if we consider the $(0\,0\,0\,1)_\alpha$ close packed plane and the $[1\,1\,\bar{2}\,0]_\alpha$ close packed direction of the α phase, six $\{1\,1\,0\}_\beta$ close packed planes may

Table 1
Nomenclature of α variants

Variant number	$(0\,0\,0\,1)_\alpha$ indices in β frame			$[1\,1\,\bar{2}\,0]_\alpha$ indices in β frame		
1	1	1	0	−1	1	−1
2	1	1	0	1	−1	−1
3	1	−1	0	1	1	−1
4	1	−1	0	−1	−1	−1
5	0	1	1	1	1	−1
6	0	1	1	−1	1	−1
7	0	1	−1	1	1	1
8	0	1	−1	−1	1	1
9	1	0	1	1	1	−1
10	1	0	1	1	−1	−1
11	1	0	−1	1	1	1
12	1	0	−1	1	−1	1

be chosen, each of them containing two $(1\,1\,1)_\beta$ close packed directions. The 12 α variants are reported in Table 1, the first two being those defined by Furuhara et al. [5]. Two stereographic projections of these 12 variants in the frame of variant 1 are presented in Fig. 3, for the lattice parameter ratio $c/a = 1.586$ of the investigated alloy [16].

These 12 possible α variants inherited from a parent β grain obey specific misorientation relationships between each other [9], which were here calculated in the form of a rotation matrix and also expressed as the minimum rotation angles and their corresponding rotation axes. To perform these calculations, an orthogonal frame with unit vectors, respectively parallel to $[2\,\bar{1}\,\bar{1}\,0]$, $[0\,1\,\bar{1}\,0]$ and $[0\,0\,0\,1]$ was defined for the α phase.

The misorientation relationships between reference variant 1 and each of the 12 α variants are reported in Table 2. These results complete those presented in Ref. [9]. In the present study, they are used as a means to recognise the α variants related to the same parent β grain.

3.2. *Habit plane of the α phase*

The study of interfaces, and more particularly the characterisation of grain boundaries in polycrystals, is a major application of EBSD. Different ways of investigation are reported in literature. EBSD data acquisition and processing relevant to interface description can be performed by collecting crystallographic orientations of adjacent grains, by serial sectioning, by analysis of two intersecting non parallel sections or by trace analysis [17]. The trace analysis method, more suited to the geometry of the investigated samples, has been used for this study.

Phase transformations of titanium and its alloys at moderate to high cooling rates are also related to the existence of particular habit planes – i.e. macroscopically invariant planes between parent and product phases – specific to the α + β type of microstructure. Blank et al. [10] addressed the martensitic bcc-to-hcp phase transformation and suggested $\{3\,3\,4\}_\beta$ and $\{3\,4\,4\}_\beta$ as habit plane indices, corresponding respectively to $\{1\,\bar{5}\,0\}_\alpha$ and $\{\bar{5}\,1\,0\}_\alpha$ in the orthogonal frame of the α phase.

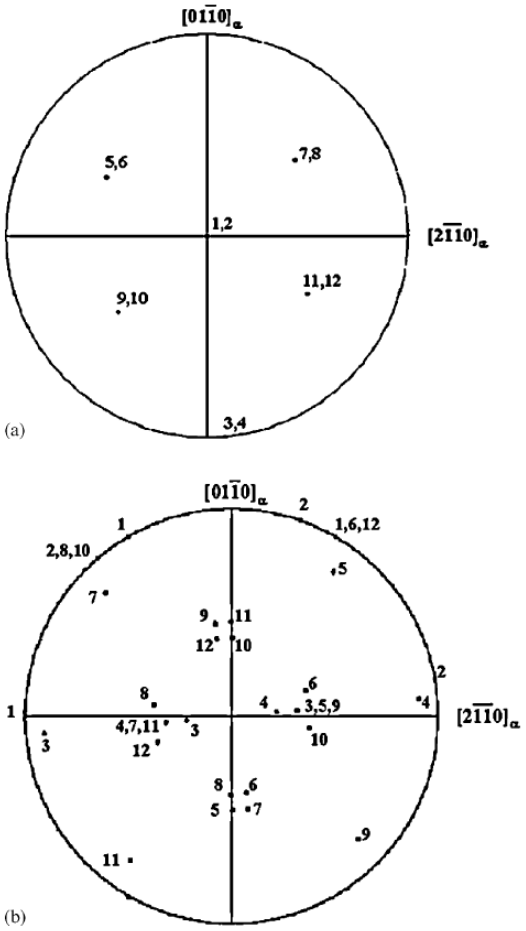

Fig. 3. (a) $\{0\,0\,0\,1\}$ and (b) $\{1\,1\,\bar{2}\,0\}$ stereographic projections of the 12 α variants in the frame of variant 1.

In the present study, the habit planes of the EBSD analysed α phase were compared to these two families of planes. First, by using the EBSD point analyses and SEM micrographs, the traces of elongated α phases in the sample plane (Fig. 1b) were mea-

Table 2
Misorientation relationships between variant 1 and any of the 12 α variants

Second variant	Misorientation angle (°)	Rotation axis
1	0.00	No rotation
2	10.53	$[0\,0\,0\,1]$ (*c*) direction
3	90.00	At +5.26° from $[2\,\bar{1}\,\bar{1}\,0]$, in the basal plane
4	90.00	At +5.26° from $[\bar{2}\,1\,1\,0]$, in the basal plane
5	60.83	At 99.03° from *c* direction, in the plane containing both (i) the *c* direction and (ii) one direction at +5.26° from $[\bar{1}\,\bar{1}\,2\,0]$ in the basal plane
6	60.00	$[\bar{1}\,\bar{1}\,2\,0]$ direction
7	63.26	At 72.44° from *c* direction, in the plane containing both (i) the *c* direction and (ii) $[\bar{1}\,2\,\bar{1}\,0]$
8	60.83	At 80.97° from *c* direction, in the plane containing both (i) the *c* direction and (ii) one direction at +5.26° from $[\bar{1}\,2\,\bar{1}\,0]$ in the basal plane
9	63.26	At 72.44° from *c* direction, in the plane containing both (i) the *c* direction and (ii) $[1\,\bar{2}\,1\,0]$
10	60.83	At 80.97° from *c* direction, in the plane containing both (i) the *c* direction and (ii) one direction at +5.26° from $[\bar{1}\,\bar{1}\,2\,0]$ in the basal plane
11	60.83	At 99.03° from *c* direction, in the plane containing both (i) the *c* direction and (ii) one direction at +5.26° from $[1\,1\,\bar{2}\,0]$ in the basal plane
12	60.00	$[1\,1\,\bar{2}\,0]$ direction

sured and expressed in the crystal frame. These experimental traces were then compared to the traces of the above mentioned possible habit planes, calculated in the crystal frame as the cross product of the plane normal by the sample normal. The angular deviation between measured and calculated traces was then determined. The accuracy of the method is about 2° despite thorough alignment procedure between the horizontal axis of the micrographs (second vector of the EBSD sample frame) and the tilt axis of the SEM.

4. Results

The results of EBSD investigations performed on filamentary titanium matrix composite are presented in two distinct parts: those related to the Ti6242S matrix and then those related to the titanium carbide phases.

4.1. Titanium matrix

4.1.1. As-processed filamentary material

The Ti6242S microstructure of the as-processed filamentary TMCs (Fig. 4) is very homogeneous and fine, so that grain boundaries are difficult to reveal. It consists in small needle or plate-shaped α crystallites of some hundreds nanometers in length, and hardly observable residual β phase. Only the parent β grain boundaries were easily determined by looking at the EBSD patterns of the β phase.

In this microstructure, EDS analyses showed that the alloying elements were homogeneously distributed throughout the matrix [18], while equilibrium conditions should lead to partitioning of the stabiliser elements in the corresponding phases. These results lead us to consider the observed microstructure to be out of equilibrium.

Due to the difficulty in observing and analysing the β phase, only one former β grain was analysed by EBSD, associated to point measurements in eight α grains in this parent β grain. The experimental α/β orientation relationships were calculated

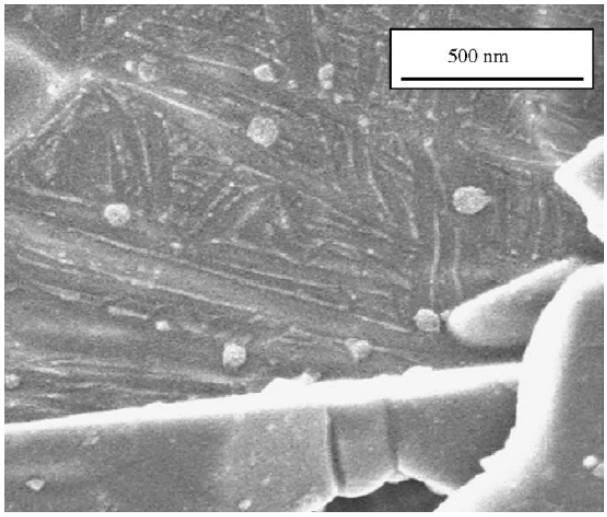

Fig. 4. As-processed filamentary material microstructure.

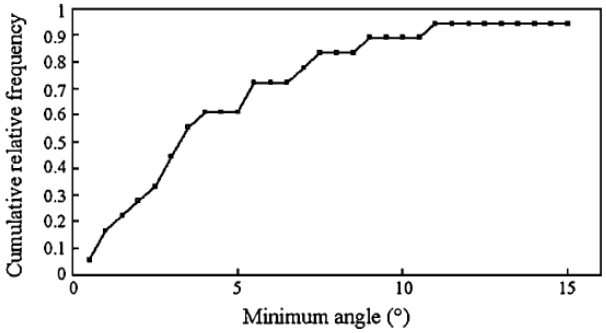

Fig. 5. Cumulative relative frequency of angular deviation between experimental and calculated traces of habit planes.

thanks to the measured Euler angles and compared with the Burgers orientation relationships. The angular deviation between experimental and calculated orientation relationships ranges between 1.3° and 3.5°, so that the actual orientation relationship is close to, but not strictly identical to α/β Burgers orientation relationships.

To enlarge the experimental database, the α/α misorientation relationships within four other former β grains were also compared with the theoretical α/α misorientation relationships between the 12 α variants inherited from the same β grain. A total of 22 α measurement points were used for this purpose. The angular deviation between experimental and theoretical misorientation relationships, θ, ranges between 0.5 and 2.5°, which falls within the usually reported tolerance of 5° [9]. Moreover, in spite of the low amount of data collected, the variety of orientations of analysed α grains does not suggest any particular variant selection during the phase transformation.

In spite of the difficult EBSD imaging conditions of this microstructure, twenty traces of elongated α phases were investigated. In the zone where the β grain could be analysed, the experimental traces were then compared with those of the {3 3 4} and {3 4 4} planes of the β crystal, whereas in the other areas the experimental traces were compared with those of the $\{1\,\bar{5}\,0\}$ and $\{\bar{5}\,1\,0\}$ planes in the orthogonal α frame (Fig. 5). The results show satisfactory agreement in both cases.

4.1.2. Heat treated filamentary material

The morphology of the α + β heat treated microstructure is similar to that of α + β forged Ti6242S alloy, with primary α grains essentially in the vicinity of the fibre/matrix interface, due to the high concentration of α stabiliser carbon. The remaining of the matrix shows elongated needle-like (or possibly plate-like) secondary α phase of some hundreds of nanometres in width and some micrometers in length, in a retained β matrix often appearing as elongated films of about 20 nm in width (Fig. 6).

EDS analyses reveal partition of alloying elements in the corresponding phases. For instance, β stabiliser molybdenum is concentrated in the β phase (Fig. 6) and α stabiliser aluminium in the α phase.

In spite of rather readily imaging of the β phase, no EBSD point measurement could be performed in this phase due to its very low thickness. Consequently, only the α/α misorientation

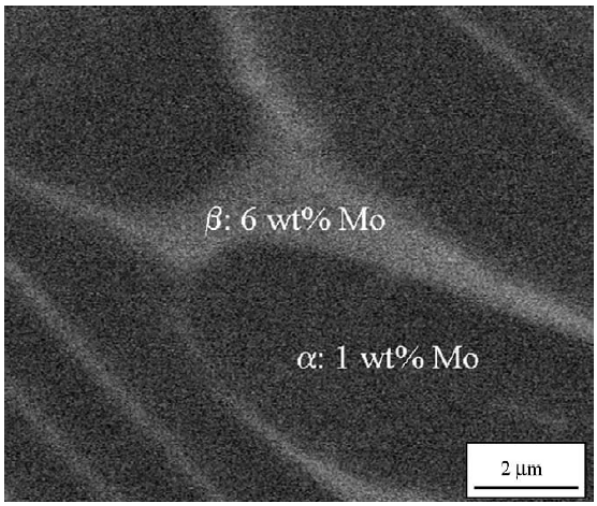

Fig. 6. Heat treated filamentary material microstructure: local EDS microanalysis of Mo content (backscattered electron imaging).

relationships were studied. From the nine measurements in α grains located in the same parent β grain, the angular deviation between experimental and theoretical α/α misorientation relationships were always lower than 3°. Furthermore, a graphical method was developed to determine the orientation of the parent β phase, by assuming that the α/β Burgers relationships are respected. The $\{0\,0\,0\,1\}$ and $\{2\,\bar{1}\,\bar{1}\,0\}$ poles figures of the α phase were plotted and the $\{0\,0\,1\}$ and $\{1\,1\,1\}$ poles figures of the parent β grain were deduced by trial and error (Fig. 7). Then, the Euler angles of the parent beta phase were determined from these pole figures. This method enables determination of the orientation of the former β phase even when it is no longer present (or too difficult to analyse by EBSD) in the material. A similar method has already been used for bainitic steels in the absence of retained austenite [19], whereas automatic methods based on direct calculations have also been developed [3,9].

4.1.3. Simulated materials

The microstructure of the as processed simulated and heat treated simulated materials reveal strong similarities with the filamentary TMCs. In fact, the as-processed simulated material possesses a very fine microstructure with α needles (or plates) of several hundreds of nanometers in length and hardly observable retained β phase (Fig. 8a). The heat treated simulated material has a β transformed microstructure with α needles (or plates) of several micrometers in length and 0.5–1 µm in width and a film-like retained β phase, resembling the microstructure of α + β forged Ti6242S alloy (Fig. 8b).

4.2. Fibre/matrix interfacial zone

4.2.1. As-processed filamentary material

During the high temperature contact between the fibre and the titanium matrix alloy in the filamentary TMC process, the high reactivity of titanium with carbon gives rise to significant carbon

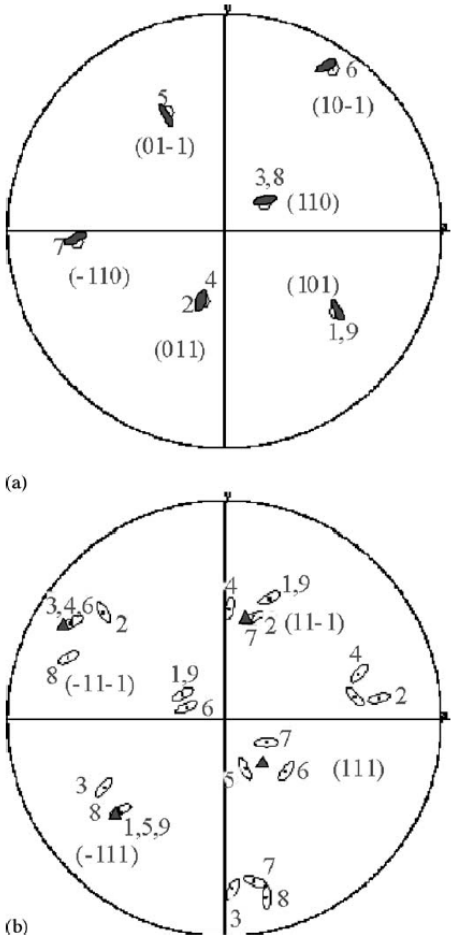

Fig. 7. (a) $\{0\,0\,0\,1\}_{\alpha}$ and $\{1\,1\,0\}_{\beta}$, and (b) $\{1\,1\,\bar{2}\,0\}_{\alpha}$ and $\{1\,1\,1\}_{\beta}$ stereographic projections of α variants and parent β grain in the heat-treated filamentary material. Open symbols and variant numbers are for the α phase; filled symbols and plane indices are for the β phase in the sample frame.

transfer from the filament toward the matrix and the formation of a brittle interfacial zone of about 10–30 µm in thickness, clearly revealed around the C coated SiC filament (Fig. 9a). In the as-processed material, this zone is composed by a titanium carbide interphase and a large outer area of Ti-based matrix with titanium carbide precipitates (black arrows in Fig. 9a). The continuous layer is about 0.5–1 µm thick, while the acicular particles range between 1 and 10 µm in length. These brittle phases constitute possible crack initiation sites and could reduce mechanical performance of the composites.

The inner layer (white arrow in Fig. 9a) consists of equiaxed grains, of 100–200 nm in size. The EBSD patterns can be indexed as for fcc crystals, suggesting the cubic TiC_{1-x} phase (which has, in fact, a NaCl crystal structure). The fracture mechanism of this brittle phase possibly depends on the misorientations between grains, so that local grain boundary misorientations were calculated thanks to the Euler angles. High angle boundaries (misorientation higher than 15°) were systematically found between adjacent grains. However, no particular texture with respect to the filamentary geometry or SiC fibre could be deduced from the

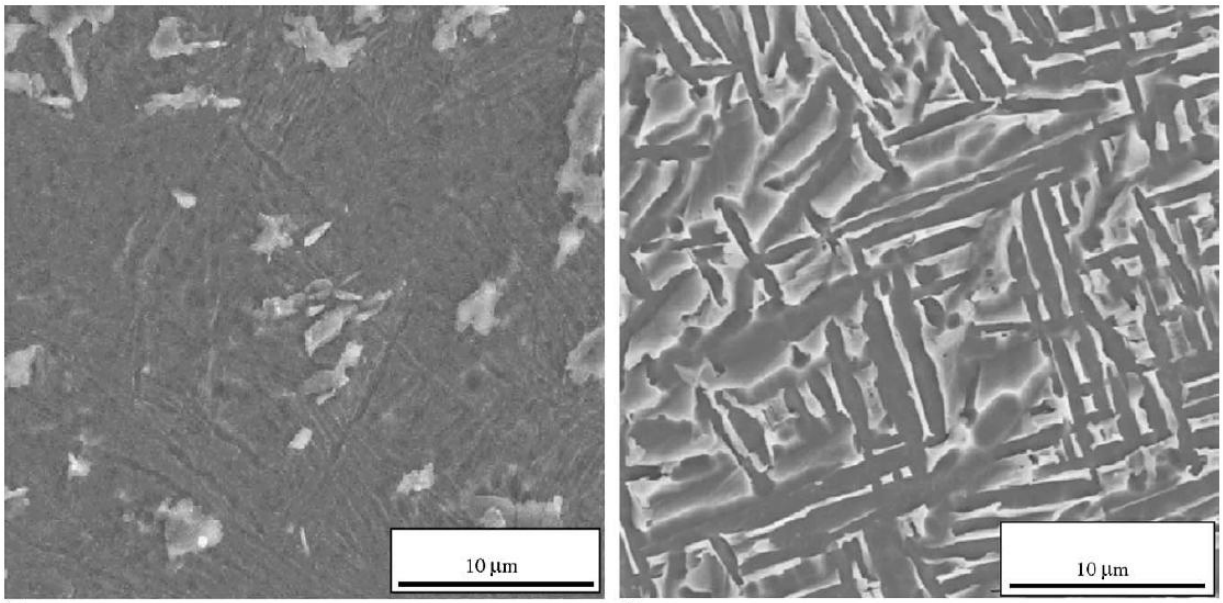

Fig. 8. Microstructure of (a) as processed and (b) heat-treated simulated materials (secondary electron imaging).

grain orientations. These results are in agreement with EBSD results obtained in a SiC_p/Ti–6Al–4V composite produced by laser melt injection, in the case when a polycrystalline TiC film is formed around SiC particles [20].

In the as-processed filamentary material, the significant volume fraction of titanium carbide phase within the interfacial zone consisted in platelets of several hundreds of nanometers in length and a few nanometers in thickness (Fig. 10a). They were located in the vicinity of the fibre/matrix interface and were determined by TEM to be sub-stoichiometric TiC_{1-x} titanium carbide [16]. Thus, the particularly rapid conditions of solidification and cooling of the Ti alloy filament coating were able to allow metastable phases formed at high temperature, such as Ti_2C, to be retained at room temperature. These results are confirmed by the Ti–C phase diagram (Fig. 2), which reveals that Ti_2C could be the titanium carbide phase present at high temperature (between 1500 and 1800 °C) for titanium matrix locally enriched in carbon up to a few atomic percents, as is the case close to the fibre. Other products of interfacial reactions such as Ti_5Si_3 were also found with TEM, in accordance with [21,22] but these particles were far too fine to be analysed with EBSD [16].

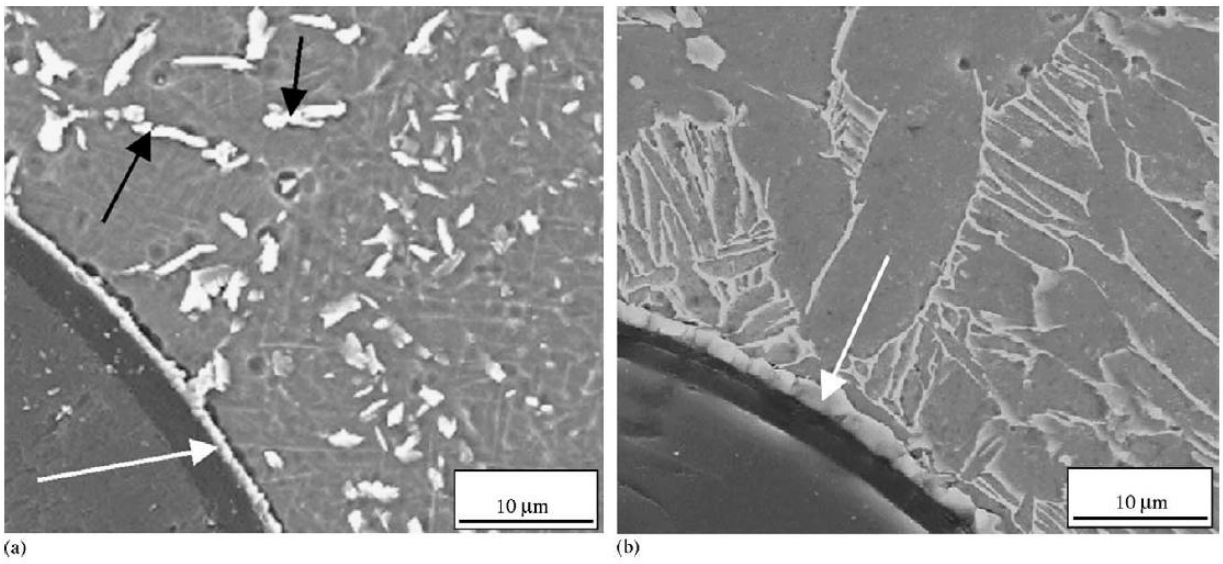

Fig. 9. Microstructure of the fibre/matrix interfacial zone: (a) as-processed filamentary material and (b) heat treated filamentary material (secondary electron imaging). Black arrows denote outer layer precipitates, white arrow denotes the inner layer.

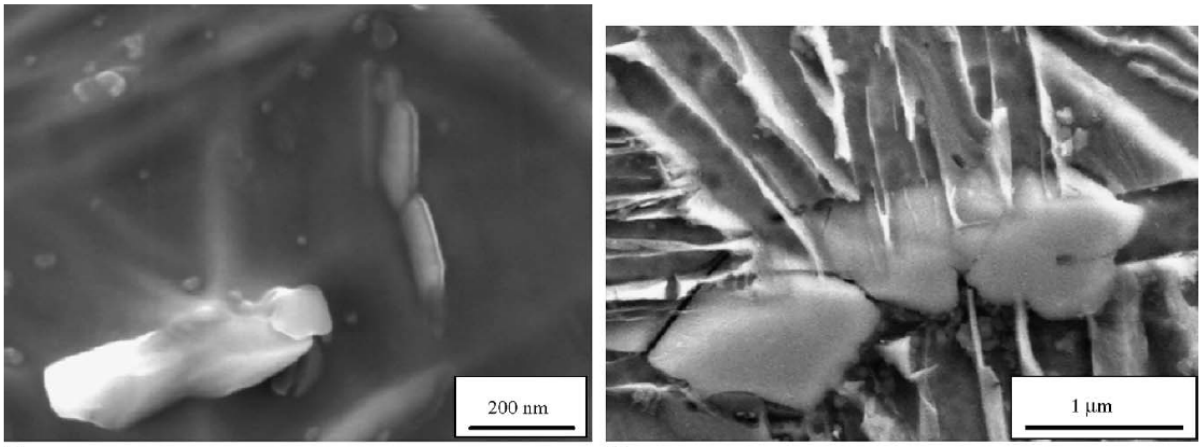

Fig. 10. Morphology of titanium carbide precipitates: (a) as-processed filamentary material and (b) as-processed simulated material.

4.2.2. *Heat-treated filamentary material*

Heat treated filamentary TMCs have a strongly modified microstructure (Fig. 9b). The thickness of the inner continuous titanium carbide layer significantly increased after the heat treatment. Within this inner layer, only high-angle boundaries (misorientation angles ranging between 35 and 51°) were found between carbide grains. Moreover, no preferred orientation of carbide crystals was evidenced with respect to the filament axes, at least on {1 0 0}, {1 1 0} and {1 1 1} pole figures.

The discontinuous precipitated carbide phase (outer layer) was no longer observed in the Ti6242S matrix. This phenomenon can be attributed to a modification of the stoichiometry of the precipitates. At high temperature the TiC_{1-x} phase in equilibrium with Ti alloy is close to $TiC_{0.5}$, whereas at temperatures around 950 °C it is closer to $TiC_{0.7}$ as supported by Fig. 2. Thus, during the heat treatment, the chemical composition of the carbide tends to be closer to stoichiometry, leading to a significant decrease in the carbide volume fraction. Moreover, rapid diffusion of carbon in the Ti alloy at temperatures close to 950 °C implies spontaneous spreading of carbon into the whole thickness of matrix coating, which can also be a source of titanium carbide phase modification. Consequently, the transferred carbon was homogeneously distributed over the matrix either as solute atoms or as sub-micrometric Ti carbide precipitates.

4.2.3. *Simulated materials*

The examination of the simulated materials allowed correlating the titanium carbide precipitate characteristics with those of the liquid route processed filamentary composites. In the as processed simulated material, precipitates were determined using Auger electron spectroscopy, SEM and TEM to be sub-stoichiometric platelets of titanium carbide with face centred cubic crystallographic structure (Fig. 10b) [16].

To examine the carbide/matrix orientation relationships before heat treatment, 37 pairs of EBSD point measurements on carbide and α neighbouring phases were collected in the simulated material in four areas corresponding to four different former β grains. In each zone, the pole figures of carbide and α phases suggest the following orientation relationships: $(1\,1\,1)_{carbide}//(0\,0\,0\,1)_{\alpha}$ and $[1\,\bar{1}\,0]_{carbide}//[2\,\bar{1}\,\bar{1}\,0]_{\alpha}$ as illustrated in Fig. 11.

After heat treatment, these precipitates were no longer observable, which confirms the evolution toward a more stable state. In equilibrium conditions, according to the Ti–C phase diagram, the mix of Ti alloy plus 0.25 wt.% C gives rise to a solid solution of carbon in the titanium alloy matrix.

5. Discussion

5.1. *Comparison between filamentary and simulated materials*

Two major differences between filamentary and simulated materials could have strongly affected the phase transformation during processing: (i) the high free surface to volume ratio of the filamentary material (300 μm in diameter, see Fig. 1); (ii) the spatial distribution of carbon-rich areas (constrained to the fibre/matrix interface in the filamentary material while more homogeneously distributed in the bulk of simulated material). In fact, no particular feature was observed near free surfaces. The only difference between filamentary and simulated materials was the former β grain size: only a few β grains were found in a single cross-section of the filamentary material, whereas Ti carbides seemed to have pinned β grain boundaries in the simulated material, leading to finer β grains and thus shorter and finer α particles.

Nevertheless, microstructural examinations of the filamentary and simulated materials reveal that the processing conditions of the simulated materials adequately reproduced the cooling conditions of the liquid route process used to manufacturing filamentary TMCs. In fact, the microstructural morphology of the Ti6242S matrix as well as the titanium carbide precipitates properties were similar both before and after heat treatment. Moreover, metallurgical modifications observed in the filamentary material after the heat treatment were in agreement with those observed on the simulated

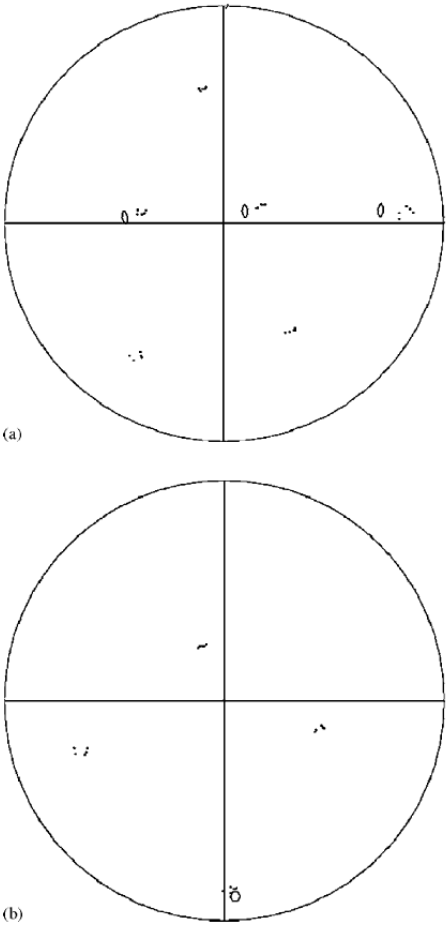

Fig. 11. Stereographic projections of titanium carbide precipitates and neighbouring α phase: (a) $\{2\,\bar{1}\,\bar{1}\,0\}_{\alpha}$ and $\{1\,1\,0\}_{carbide}$; (b) $\{0\,0\,0\,1\}_{\alpha}$ and $\{1\,1\,1\}_{carbide}$; open symbols are for the α phase; small filled squares are for the carbide phase in the sample frame.

material. Therefore, the simulated materials can be considered as a reliable representation of the filamentary materials and could be used for further characterisation with easier sample preparation than for filamentary materials.

5.2. *Phase transformations in the rapidly cooled materials*

At the matrix/fibre interface, the particularly rapid conditions of solidification and cooling of the filamentary titanium matrix composites give rise to a metastable state characterised by the presence of sub-stoichiometric TiC_{1-x} titanium carbide precipitates. In fact, numerical calculations showed that the cooling rate ranges between 1000 and 1600 °C/s, depending on processing conditions [16].

The microstructural properties of the Ti6242S matrix are strongly influenced by processing conditions. The very fine microstructure obtained in the as-processed filamentary TMC and the absence of partition of alloying elements lead us to consider that the β → α phase transformation should proceed by cooperative displacements of atoms. The comparison of the habit plane of the EBSD analysed α phase with results of Blank et al. [10] emphasized that the experimental traces are in agreement with theoretical ones. This, together with the near-Burgers orientation relationships and the plate-like morphology, tends to postulate the martensitic type of the β → α phase transformation in these conditions (in contrast with e.g. a massive transformation mechanism).

5.3. *Evaluation of the investigation method*

The filament/matrix interface is hardly observable by classical characterisation methods. Even if some TEM observations have been carried out, thin foil preparation is difficult because of (i) a high difference in hardness between silicon carbide filament and titanium alloy matrix; (ii) the small diameter (around 300 μm) of the filamentary materials. With easier sample preparation, EBSD analyses allowed pointing out the cubic crystal structure and the absence of texture of titanium carbide phase at the filament/matrix interface. Moreover, misorientations between TiC_{1-x} grains, evaluated to be higher than 15°, might be useful to further investigate the fracture mechanisms of TMCs.

6. Conclusions

EBSD investigations associated with high-resolution SEM of filamentary titanium matrix composites pointed out the crystallographic properties of the fine-scale titanium alloy and interfacial microstructure. The microstructural specificities of these as-processed filamentary materials could be accurately simulated on bulk materials.

After processing and rapid cooling of the filamentary TMCs, the titanium alloy matrix characterisation reveals a α dominated martensitic microstructure and metastable titanium carbides. The filament/matrix interface consists of small randomly oriented grains of sub-stoichiometric TiC_{1-x} titanium carbides.

The heat treated filamentary TMCs possess a more stable matrix microstructure similar to that of α + β forged Ti6242S alloy, with elongated α colonies maintaining a near-Burgers orientation relationship with the former β phase. The inner layer of the fibre/matrix interface grows by carbon diffusion from the SCS-6 filament toward the titanium alloy matrix while the carbides located in the outer layer disappear.

Acknowledgements

This work was part of research activities founded by Snecma Company. Support from the Ceramic Materials and Metallic Matrix Composites group of the ICMCB Institute (CNRS-Bordeaux University), and from the EPM Madylam Laboratory (CNRS-Grenoble) is gratefully acknowledged.

References

[1] J. Humphreys, Scr. Mater. 51 (2004) 771–776.
[2] A.F. Gourgues, Mater. Sci. Technol. 18 (2002) 119–133.

[3] M.G. Glavicic, P.A. Kobryn, T.R. Bieler, S.L. Semiatin, Mater. Sci. Eng. A 351 (2003) 258–264.
[4] M.G. Glavivic, P.A. Kobryn, T.R. Bieler, S.L. Semiatin, Mater. Sci. Eng. A 346 (2003) 50–59.
[5] T. Furuhara, T. Maki, Mater. Sci. Eng. A 312 (2001) 145–154.
[6] M. Humbert, N. Gey, J. Appl. Crystallogr. 35 (2002) 401–405.
[7] M. Humbert, H. Moustahfid, F. Wagner, M.J. Philippe, Scr. Metall. Mater. 30 (1994) 377–382.
[8] N. Stanford, P.S. Bate, Acta Mater. 52 (2004) 5215–5224.
[9] N. Gey, M. Humbert, J. Mater. Sci. 38 (2003) 1289–1294.
[10] V.D. Blank, B.A. Kulnitskiy, Scr. Mater. 37 (1997) 373–376.
[11] F. Zimmermann, M. Humbert, Acta Mater. 50 (2002) 1735–1740.
[12] N. Gey, M. Humbert, Acta Mater. 50 (2002) 277–287.
[13] N. Carrère, D. Boivin, R. Valle, A. Vassel, Scr. Mater. 44 (2001) 867–872.
[14] B. Dambrine, M. Garnier, J. Hamburger, Y. Honnorat, L. Molliex. Procédé d'enduction métallique de fibres par voie liquide. French Patent # 2773820(9800644), 1998 (in French).
[15] T.B. Massalski, Binary Alloy Diagrams, 2nd ed., American Society for Metals, Materials Park, OH, 1990, pp. 888–891.
[16] C. Duda, Description and improvement of high speed coating conditions related to silicon carbide filaments/titanium alloy coupling. PhD dissertation, Université Bordeaux I, France, 2004. http://tel.ccsd.cnrs.ft/tel-00012140 (in French).
[17] V. Randle, Int. Mater. Rev. 49 (2004) 1–11.
[18] C. Duda, C. Arvieu, J.F. Fromentin, J.M. Quenisset, Compos. Part A: Appl. Sci. Manuf. 35 (2004) 511–517.
[19] A.F. Gourgues, H.M. Flower, T.C. Lindley, Mater. Sci. Technol. 16 (2000) 26–40.
[20] Y.T. Pei, V. Ocelik, J.Th.M. DeHosson, Acta Mater. 50 (2002) 2035–2051.
[21] Y.Q. Yang, Y. Zhu, Z.J. Ma, Y. Chen, Scr. Mater. 51 (2004) 385–389.
[22] B.J. Kooi, M. Kabel, A.B. Kloosterman, J.Th.M. DeHosson, Acta Mater. 47 (1999) 3105–3116.